IOPscience iopscience.iop.org

Home Search Collections Journals About Contact us My IOPscience

Isomeric mirror states as probes for effective charges in the lower pf shell

This article has been downloaded from IOPscience. Please scroll down to see the full text article.

2011 J. Phys. G: Nucl. Part. Phys. 38 035104

(http://iopscience.iop.org/0954-3899/38/3/035104)

View the table of contents for this issue, or go to the journal homepage for more

Download details:
IP Address: 140.181.66.4
The article was downloaded on 22/05/2012 at 15:26

Please note that terms and conditions apply.

J. Phys. G: Nucl. Part. Phys. **38** (2011) 035104 (17pp) doi:10.1088/0954-3899/38/3/035104

Isomeric mirror states as probes for effective charges in the lower pf shell

R Hoischen[1,2], D Rudolph[1], H L Ma[1,3], P Montuenga[1], M Hellström[1], S Pietri[2,4], Zs Podolyák[4], P H Regan[4], A B Garnsworthy[4,5,12], S J Steer[4,13], F Becker[2,14], P Bednarczyk[2,6], L Cáceres[2,7], P Doornenbal[2,8,15], J Gerl[2], M Górska[2], J Grębosz[2,6], I Kojouharov[2], N Kurz[2], W Prokopowicz[2], H Schaffner[2], H J Wollersheim[2], L-L Andersson[1,16], L Atanasova[9], D L Balabanski[9,10], M A Bentley[11], A Blazhev[8], C Brandau[2,4], J R Brown[11], C Fahlander[1], E K Johansson[1] and A Jungclaus[7]

[1] Department of Physics, Lund University, S–22100 Lund, Sweden
[2] GSI Helmholtzzentrum für Schwerionenforschung mbH, D–64291 Darmstadt, Germany
[3] Department of Nuclear Physics, China Institute of Atomic Energy, Beijing 102413, People's Republic of China
[4] Department of Physics, University of Surrey, Guildford, GU2 7XH, UK
[5] Wright Nuclear Structure Laboratory, Yale University, New Haven, CT 06520-8124, USA
[6] The Henryk Niewodniczański Institute of Nuclear Physics (IFJ PAN), PL–31-342 Kraków, Poland
[7] Departamento de Fisica Teórica, Universidad Autonoma de Madrid, E-28049 Madrid, Spain
[8] Institut für Kernphysik, Universität zu Köln, D–50937 Köln, Germany
[9] Faculty of Physics, University of Sofia, BG–1164 Sofia, Bulgaria
[10] Institute for Nuclear Research and Nuclear Energy, Bulgarian Academy of Sciences, BG-1784 Sofia, Bulgaria
[11] Department of Physics, University of York, York, YO10 5DD, UK

E-mail: Robert.Hoischen@nuclear.lu.se

Received 7 September 2010
Published 18 January 2011
Online at stacks.iop.org/JPhysG/38/035104

Abstract

Following the fragmentation of a 550 MeV u^{-1}primary beam of ^{58}Ni, time- and energy-correlated γ decays from isomeric states in neutron-deficient nuclei in the $1f_{7/2}$ shell have been identified using the GSI fragment separator in combination with the RISING Ge-detector array. The results on isomers in the mirror pairs $^{43}_{22}Ti_{21}$–$^{43}_{21}Sc_{22}$ ($I^\pi = 3/2^+$ and $19/2^-$), $^{45}_{24}Cr_{21}$–$^{45}_{21}Sc_{24}$ ($I^\pi = 3/2^+$) and $^{45}_{23}V_{22}$–$^{45}_{22}Ti_{23}$ ($I^\pi = 3/2^-$) are discussed in the framework of large scale

[12] Present address: TRIUMF, Vancouver, British Colombia V6T 2A3, Canada
[13] Present address: Department of Engineering, Cambridge University, Cambridge, CB2 1PZ, UK
[14] Present address: FZ Karlsruhe, D-76344 Eggenstein, Germany
[15] Present address: RIKEN, Saitama 351-0198, Japan
[16] Present address: University of Liverpool, Liverpool L69 7ZE, UK

0954-3899/11/035104+17$33.00 © 2011 IOP Publishing Ltd Printed in the UK & the USA

pf and sdpf shell-model calculations, the former in conjunction with isospin symmetry breaking effects with emphasis on effective charges.

(Some figures in this article are in colour only in the electronic version)

1. Introduction

Isomeric or metastable states have been and continue to be valuable sources for probing nuclear structure models [1]. In many cases they provide the first profound glimpse of excited states in nuclei far from the line of β-stability and thus pave the way for further, more comprehensive studies at the edge of nuclear existence. Modern experimental approaches have become sufficiently sensitive to discriminate isomeric states based on samples of sometimes less than a thousand synthesized nuclei of a given species—at least as long as they can be provided and identified as isotopically pure samples [2–6].

Isomeric states are common in the vicinity of doubly-magic nuclei, i.e. isotopes for which both proton and neutron numbers are near closed shells. Thereby they probe the nuclear interaction used to describe these fix points of the spherical shell model at the same time as they provide severe constraints on the respective parameter sets. In particular, they probe excitation energies and electromagnetic decay properties of states, which are, for example, based on couplings of one or few holes in shells below a magic gap with one or a few particles situated in shells above a magic gap.

For self-conjugate nuclei as well as for neighbouring isotopes the isospin degree of freedom can be efficiently probed, i.e. to which extent the charge symmetry and charge independence of the strong force holds inside the nuclear medium, though isospin symmetry is naturally broken by the electromagnetic force. In this respect so-called mirror isomers play a crucial role—these are isobaric analogue states with the same quantum numbers but in nuclei, which have the number of protons and neutrons interchanged. Early experimental studies were already performed decades ago on isomeric spin $I^{\pi} = 19/2^{-}$ isobaric analogue states in the mass $A = 43$, $T_z = \pm 1/2$ mirror pair ^{43}Sc and ^{43}Ti [7, 8]. These isobars possess one proton and two neutrons or one neutron and two protons outside the doubly-magic $N = Z = 20$ ^{40}Ca core, respectively, i.e. their low-lying negative-parity states are expected to be dominated by rather pure $1f_{7/2}{}^{3}$ configurations.

Furthermore, isomeric $3/2^{+}$ states are reported well below the pairing gap in both ^{43}Sc and ^{43}Ti. They are found to essentially decay by magnetic quadrupole, $M2$, γ-ray transitions into the respective $7/2^{-}$ ground states [9]. The underlying leading structure of such $3/2^{+}$ states involves $1d_{3/2}{}^{-1} \times [1f_{7/2}{}^{4}]_0$ partitions, for which the anti-aligned proton–neutron coupling in the $1f_{7/2}$ shell is thought to be responsible for re-gaining the energy of exciting a nucleon across the shell gap at particle number 20 [9, 10]. Mainly owing to limited computational power, these early studies invoked rather limited shell-model configuration spaces, and Coulomb displacement energies of isobaric analogue states were rather discussed on a macroscopic and systematic level [9, 11].

Recent years have seen significant steps taken towards the microscopic understanding of 'mirror energy differences' (MED), i.e. differences in excitation energies of analogue states, in a number of $T_z = \pm 1/2$ mirror pairs and $T_z = 0, \pm 1$ isospin triplets located between ^{40}Ca and ^{56}Ni on the chart of nuclei [12], and also beyond ^{56}Ni [13, 14]. Proper descriptions of MED sequences in these pf-shell nuclei call for an isospin breaking part in the strong force [12, 15], and there is an overall excellent quality of agreement in this mass regime between experiment and predictions based on modern large-scale shell-model approaches—with only

few exceptions as pointed out in, for example, [16–18]. There have also been first attempts of shell-model calculations in larger model spaces, i.e. coupling $1d_{3/2}$ particles to the pf shell [19] with significant progress towards full sd–pf calculations within the spherical shell-model and approaches based on density functional theory [20]. These theoretical descriptions provided very good agreement with recent experimental high-spin data [21, 22].

Similar to these $1d_{3/2}$ 'extruder' states in the lower half of the $1f_{7/2}$ shell, $1g_{9/2}$ 'intruder' states readily occur in the upper half of the $1f_{7/2}$ shell below the doubly-magic $N = Z = 28$ nucleus ^{56}Ni [23–25]. However, the inclusion of either the full sd, the $1d_{3/2}$ or the $1g_{9/2}$ shell to the usually very successful 'pure' pf shell-model space does not only cause a significant increase in the dimensions of the Slater determinants to be diagonalized, but also induces technical problems within the prescriptions of the spherical shell model [26].

In fact, it is an ongoing challenge for modern isospin-dependent large-scale shell-model descriptions to properly describe mirror isomers in nuclei located in the $1f_{7/2}$ shell—not only in terms of excitation energy, but moreover by means of dynamic and static electromagnetic moments. The aim of this work is to re-iterate the process based on revised and new experimental results combined with recent shell-model developments. Section 2 presents some details of the experimental approach. In section 3 the data analysis is described and the partially new and partially refined results on isomeric mirror states in the lower half of the $1f_{7/2}$ shell are summarized. They are discussed in the framework of contemporary large-scale shell-model calculations in section 4.

2. Experimental approach

A unique method to correlate the γ radiation from isomeric states with a given isotope involves the production of rare isotopes by fragmentation reactions followed by separation, event-by-event identification and implantation of the residues in the focus of a Ge-detector array. The present experiment was performed within the *Rare Isotope Spectroscopic Investigations at GSI* (RISING) campaign. Here, isomeric states in the nuclei of interest were populated by the fragmentation of a ^{58}Ni primary beam at 550 MeV u^{-1} impinging on a 4 g cm^{-2} Be target. The beam was provided by the UNILAC-SIS accelerator complex at the GSI Helmholtzzentrum für Schwerionenforschung mbH, Darmstadt, Germany. The reaction products subsequently entered the roughly 70 m long *fragment separator* (FRS) [27]. Because of the high kinetic energies and relatively low mass, both beam particles and residues travelled with charge states $Q = Z$, i.e. with the transmitted ions being fully stripped of atomic electrons.

The FRS separation scheme is based on a $B\rho - \Delta E - B\rho$ sequence [27] and, generally speaking, foresees the transport of a certain, selected portion of the chart of nuclei from the radiation hot target spot to the radiation cool final focus. Figure 1 provides the identification plot of the nuclides identified in this work. These are in total 24 $N \leqslant Z$ nuclides with proton numbers ranging from potassium, $Z = 19$, to manganese, $Z = 25$. For each entry in figure 1 a restrictive use of the full suite of signals from scintillator and ionization detectors placed at the intermediate and final focii of the FRS has been made [27–29]. In this way of complete tracking, a total of 1.17 million fragments can be uniquely identified.

In the offline analysis it was noted that many events (and in particular those associated with the lighter fragments) were missing proper tracking information from two multi-wire detector systems. This can be attributed to a too low gas pressure, i.e. the lesser ionizing lighter fragments produced too small signals to surpass the threshold level of the associated electronics. Nevertheless, it is possible to recover almost all of these events, because for light nuclei the time-of-flight measurement between the intermediate and the final focus of the FRS turned out to be sufficiently precise to distinguish the A/Z ratio for a given element, with

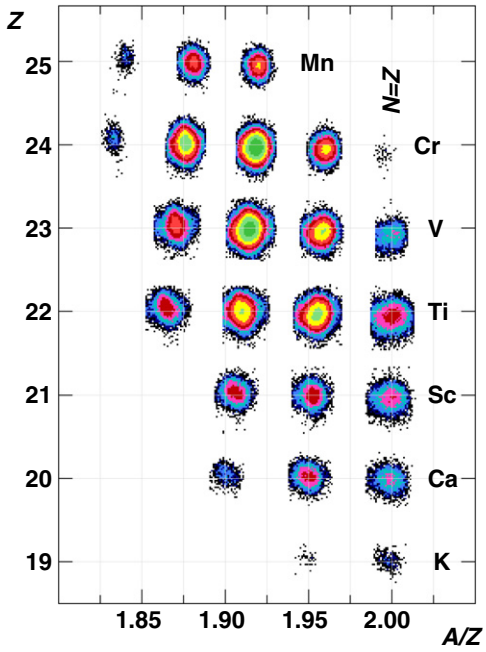

Figure 1. Identification plot of $N \leqslant Z$ nuclides produced in the fragmentation of a ^{58}Ni beam on a ^{9}Be target. The proton number, Z, is plotted versus the mass-over-charge ratio, A/Z, for fragments, which passed the FRS and its full suite of tracking, time-of-flight and energy loss detection systems.

the Z separation provided independently using the ion energy losses in the MUSIC detectors (cf figure 1). In a next step, events lacking complete tracking information are identifiable by considering the average track of a given isotope species, which can be easily derived from the 1.17 million completely determined events. This leads ultimately to an identification plot similar to figure 1, but with almost five times more entries, namely 5.38 million 'partially tracked' ones [29]. Thereby the 'gain factors' varied strongly between about 2 for the heavier Mn or Cr fragments up to about 100 for the lighter Ca isotopes.

Following the deceleration in an aluminum degrader and a survival check in a plastic scintillator placed behind this degrader, the fragments were ultimately stopped in a 12 mm thick piece of plastic, which was positioned in the centre of the RISING γ-ray detector array. For the present experiment, the travel time of the nuclei of interest from the primary beryllium fragmentation target to this implantation point amounts to some 350 ns. Note, however, that electromagnetic decays via inner conversion are prohibited during the flight, since the fragments are bare nuclei.

The RISING array itself comprises 15 high-resolution and high-efficiency CLUSTER germanium detectors [30], each consisting of seven large-volume Ge-detector crystals. The 105 Ge-detector signals were each divided into two separate branches. The first branch was read out by digital electronics providing the energy and the timing of the γ-ray events, the latter in steps of 25 ns with respect to the trigger signal. This signal was generated by each ion passing through the first fast plastic scintillation detector positioned in the final FRS focal plane area. The second branch employed a conventional sequence of timing electronics, namely a fast amplification stage followed by constant fraction discrimination and time-to-digital converters with a resolution of less than 1 ns per digitized channel. The data

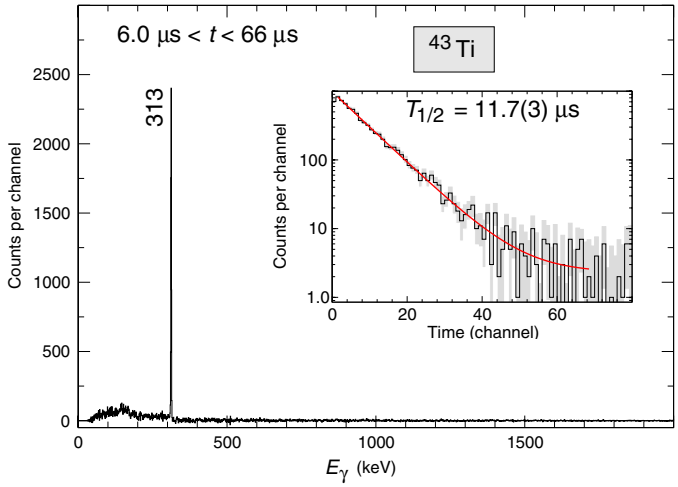

Figure 2. Gamma-ray spectrum taken between 6.0 and 66 μs after the implantation of ^{43}Ti ions. The peak is labelled with its energy in keV. The inset shows the decay curve of the 313 keV transition in ^{43}Ti. The experimental data are histogrammed in bins of 2 μs per channel, and the grey area marks the experimental uncertainties. The solid line corresponds to the result of a least-squares fitting procedure to the exponential decay, including a constant background term.

acquisition system had a selected waiting time of up to 200 μs after a trigger signal, before it reset and would accept a trigger from another fragment. The events were stored in listmode on computer hard disks, comprising the encoded information of the FRS detectors and time and energy of the correlated, prompt and delayed γ rays. More information on the experiment and the respective RISING setup can be found in [28, 29, 31].

3. Analysis and results

In the beginning of the analysis, the 'partially tracked' data set was employed to inspect γ-ray spectra, which are correlated with a preceding implantation of one of the 24 ion species displayed in figure 1. Different generic ranges for the correlation time period after the implantation have been investigated, focusing on isomeric γ decay in the few-hundred nanosecond, several microsecond, and several tens of microsecond regimes. Since the γ-ray spectra related to the relatively abundant isotopes ^{44}V (9.4×10^5 implantations) and ^{46}Cr (7.5×10^5 implantations) do not show any sign of isotope-correlated delayed γ rays, i.e. isomeric states, normalized summed γ-ray spectra of these two nuclides serve as background references. Note that different time ranges yield different γ-ray background spectra for figures 2, 3, 5 and 6.

The comparison of isotope specific γ-ray spectra with these background reference spectra gives rise to the confirmation of established isomers in the odd–odd $N = Z$ nuclei ^{38}K - $(7)^+$ state at 3458 keV, $T_{1/2} = 21.95(11)$ μs, [32, 33] - and, very weakly due to the long half-life, ^{46}V - 3^+ state at 801 keV, $T_{1/2} = 1.02(7)$ ms, [34, 35]. The procedure leads further to the observation and improvement of the knowledge of isomers in the $N = Z - 1$, $T_z = -1/2$ nuclei ^{43}Ti - $(3/2^+)$ state at 313 keV, $T_{1/2} = 12.6(6)$ μs, [9, 36]; $(19/2^-)$ at 3066 keV, $T_{1/2} = 560(6)$ ns, [7, 8, 36] - and ^{45}V - $(3/2^-)$ at 57 keV, $T_{1/2} = 0.43(8)$ μs, [10, 37]. Finally, evidence was found for a previously unreported long-lived isomeric state in the exotic $N = Z - 3$, $T_z = -3/2$ nucleus ^{45}Cr.

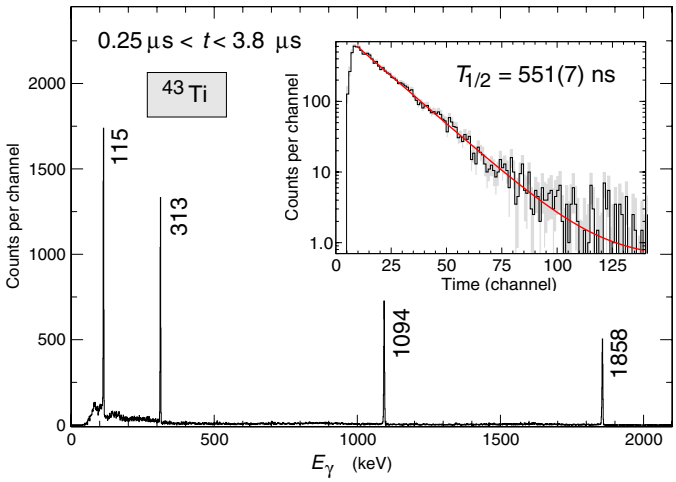

Figure 3. Gamma-ray spectrum taken between 0.25 and 3.8 μs after the implantation of ^{43}Ti ions. The peaks are labelled with their energy in keV. The inset shows the combined decay curve of the 115, 1094 and 1858 keV transitions in ^{43}Ti. The experimental data are histogrammed in bins of 50 ns per channel including an arbitrary offset. The grey area marks the experimental uncertainties. The solid line corresponds to the result of a least-squares fitting procedure to the exponential decay, including a constant background term.

Figure 2 illustrates the method of combining isotopically selected sources and high-resolution γ-ray spectroscopy: the spectrum is correlated with 6.1×10^5 ^{43}Ti nuclei in the time range between 6.0 and 66 μs after their implantation. Long-lived background radiation has been accounted for in the way described above. Since the lower time limit amounts to more than ten half-lives of the $19/2^-$ isomer in ^{43}Ti, the resulting γ-ray spectrum in figure 2 contains exactly one peak at 313 keV. This peak identifies the decay of an isomeric $3/2^+$ state at 313 keV excitation energy. The inset shows the decay curve of the γ-ray transition at 313 keV. A least-squares fit to the data points yields a half-life of $T_{1/2} = 11.7(3)$ μs, which is somewhat lower than but still consistent with the literature value of $T_{1/2} = 12.6(6)$ μs [9, 36].

A decay function $f(t) = A_0 \cdot \exp(A_1 t) + A_2$ has been chosen, and the best values of the three parameters A_0, A_1 and A_2 are found by a χ^2 minimization on a fine three-dimensional grid. The experimental uncertainties of the spectrum in the inset of figure 2 are taken into account. The uncertainty of one specific coefficient is found by stepping away from its optimum value until $\chi^2 = \chi^2{}_{\min} + 1$, while varying the respective other two parameters.

The origin of the γ-ray spectrum in figure 3 is essentially the same as the one in figure 2. The only difference is that the time window is moved to somewhat shorter times, 0.25 μs $< t <$ 3.8 μs. This spectrum thus focuses on the $19/2^-$ isomer in ^{43}Ti and its cascading $E2$ decay towards the $7/2^-$ ground state via the γ-ray lines at 115, 1094, and 1858 keV. (The peak at 313 keV in figure 3 stands for decays associated with the early decays of the microsecond isomer discussed above.) The inset of figure 3 uses the full statistics of the cascade and shows the combined decay curve of the 115, 1094 and 1858 keV transitions. The present half-life result, $T_{1/2} = 551(7)$ ns, is consistent with the literature [7, 8, 36]. For reference, the isomeric decay scheme of ^{43}Ti is given in figure 4 with the adopted half-life values and suggested spins and parities of the excited states [36]. The numerical results are summarized in table 1.

Figure 5 provides the background subtracted γ-ray spectra correlated with 2.2×10^5 implanted ^{45}V ions. One transition at 57 keV is observed, corresponding to the decay of the previously reported $(3/2^-)$ level at 56.4 keV excitation energy [10, 37]. The half-life deduced

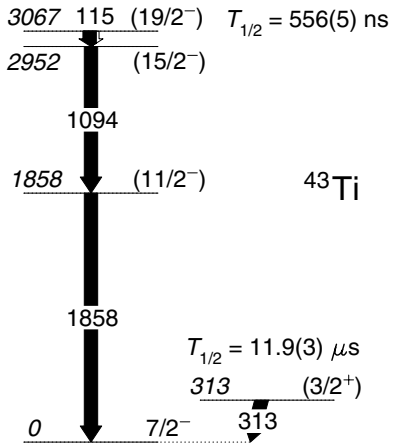

Figure 4. Decay scheme of the two isomeric states established in ^{43}Ti. The half-life values resemble the adopted values presented in table 1.

from the decay curve shown in the inset of figure 5 amounts to $T_{1/2} = 468(23)$ ns, which is consistent with the result obtained in [10], namely $T_{1/2} = 0.43(8)$ μs.

A previously unreported and rather long-lived isomeric state is observed in the exotic $T_z = 3/2$ isotope ^{45}Cr. Figure 6 shows the experimental result. Clearly, there is a peak at 107 keV in the background-free γ-ray spectrum, which is correlated with the implantation of some 2.9×10^5 ^{45}Cr nuclei. Nevertheless, the decay spectrum in the inset has considerably less statistics than in the previous, less exotic cases. In addition, the number of counts appears to increase again some 130–150 μs after implantation. The physics explanation would be statistical fluctuations of the decay of a quite long-lived ($T_{1/2} \rightarrow$ ms) state. A technical explanation could lie in the functioning of the digital electronics modules, which at read-out time provide the first measured γ-ray energy (here: 107 keV) following the trigger signal, but with the timing of the latest processed signal. The trigger rate of the experiment of some 5000 per second implies an average time difference between two subsequent ions of about 200 μs. This may lead to events with a transition of 107 keV energy being properly correlated with ^{45}Cr ions but with times related to γ radiation from subsequently implanted ions being processed in the same electronics module. The lower limit of $T_{1/2} > 80$ μs for the isomer in ^{45}Cr is thus derived from ion-γ correlations occurring within the first 80 μs after implantation or trigger signal, respectively.

^{45}Sc is the stable mirror nucleus of ^{45}Cr. A long-lived, $T_{1/2} = 318(7)$ ms, isomeric $3/2^+$ state is established as low as at $E_x = 12.4$ keV excitation energy above the $7/2^-$ ground state. The second excited state in ^{45}Sc is known to have $I^\pi = 3/2^-$ at $E_x = 377$ keV with a half-life of $T_{1/2} = 43.3(23)$ ps [37]. With these two states being the only ones known in ^{45}Sc with $T_{1/2} > 10$ ps, and given a reliably measured ground-state spin and parity of $I^\pi = 7/2^-$ for ^{45}Cr [38], the present new isomeric state in ^{45}Cr can be associated with either the $3/2^-$ or $3/2^+$ mirror state in ^{45}Sc. Therefore, the present experimental result on ^{45}Cr is quoted twice in table 1 to allow for a discussion of both options in section 4.

The transition strengths provided in table 1 are derived using the following equations (see, for example, chapter 2.3 in [40]):

$$B(M2) = \frac{b}{1+\alpha_{\mathrm{tot}}} \cdot \frac{0.051\,33}{T_{1/2}E_\gamma^5}, \qquad B^W(M2) = B(M2)/1.65 \cdot A^{2/3} \tag{1}$$

Table 1. Experimental results on excitation energies, spins, parities and half-lives of the isomeric states and γ-ray energies, multipolarities and strengths of the transitions depopulating the isomers.

	E_x (keV)	I^π ($\hbar$)	$T_{1/2}$ Present	$T_{1/2}$ Previous [36, 37]	$T_{1/2}$ Adopted	E_γ (keV)	Multi-polarity	α_{tot} Experimental [36, 37]	α_{tot} Calculated [39]	$B(T\lambda)$ (W.u.)
^{43}Sc	151	$3/2^+$		438(7) μs	438(7) μs	151.6(2)	$M2$	0.041(4)	0.0406(6)	0.069(2)[a]
^{43}Ti	313	$(3/2^+)$	11.7(3) μs	12.6(6) μs	11.9(3) μs	312.7(2)	$(M2)$	–	0.0048(1)	0.071(2)
^{43}Sc	3123	$19/2^-$		470(4) ns	470(4) ns	135.8(2)	$E2$	–	0.093(1)	2.67(4)
^{43}Ti	3066	$(19/2^-)$	551(7) ns	560(6) ns	556(5) ns	114.7(2)	$(E2)$	–	0.200(3)	4.78(10)
^{45}Sc	12.4	$3/2^+$		318(7) ms	318(7) ms	12.4($\frac{1}{2}$)	$M2$	632(71)	416(15)	0.042($^{10}_{6}$)[a]
^{45}Cr	107	$(3/2^+)$	$> 80\,\mu$s		$> 80\,\mu$s	107(1)	$(M2)$	–	0.215(8)	< 1.9
^{45}Sc	377	$3/2^-$		43.3(23) ps	43.3(23) ps	377.1(4)	$E2$	–	~ 0	15(1)
^{45}Ti	36.7	$3/2^-$		3.0(2) μs	3.0(2) μs	36.7(2)	$E2$	10(8)	16.6(3)	17(2)
^{45}V	57.1	$(3/2^-)$	468(23) ns	430(80) ns	465(22) ns	57(1)	$(E2)$	–	3.34(25)	22(5)[b]
^{45}Cr	107	$(3/2^-)$	$> 80\,\mu$s		$> 80\,\mu$s	107(1)	$(E2)$	–	0.319(13)	< 0.05

[a] Derived using the measured conversion coefficient.

[b] Assuming a branching ratio of 0.45 [37].

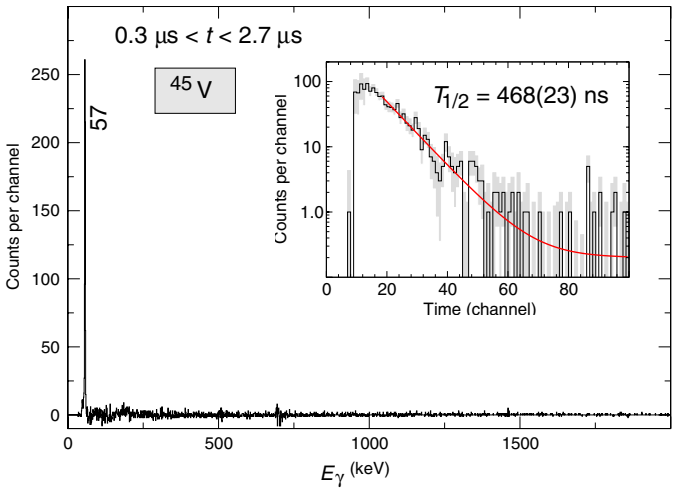

Figure 5. Gamma-ray spectrum taken between 0.3 and 2.7 μs after the implantation of ^{45}V ions. The peak is labelled with its energy in keV. The inset shows the decay curve of the 57 keV transition in ^{45}V. The experimental data are histogrammed in bins of 75 ns per channel including an arbitrary offset. The the grey area marks the experimental uncertainties. The solid line corresponds to the result of a least-squares fitting procedure to the exponential decay, including a constant background term.

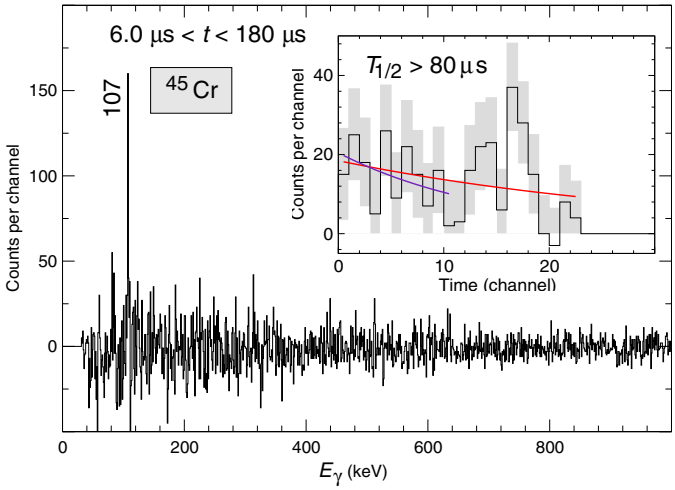

Figure 6. Gamma-ray spectrum taken between 6.0 and 180 μs after the implantation of ^{45}Cr ions. The peak is labelled with its energy in keV. The inset shows the decay curve of the 107 keV transition in ^{45}Cr. The experimental data are histogrammed in bins of 8 μs per channel, and the grey area marks the experimental uncertainties. The solid lines correspond to the result of least-squares fitting procedures to a presumed exponential decay plus constant background in the range 0–80 μs and 0–180 μs.

and

$$B(E2) = \frac{b}{1+\alpha_{\mathrm{tot}}} \cdot \frac{566.1 \times 10^{-6}}{T_{1/2} E_\gamma^5}, \quad B^W(E2) = B(E2)/0.0594 \cdot A^{4/3}. \qquad (2)$$

Here, b denotes the branching ratio and α_{tot} the total conversion coefficient of the γ-ray transition. Half-lives, $T_{1/2}$, are in μs and γ-ray energies, E_γ, in MeV. $B(M2)$-values are in

units of $\mu_N{}^2\text{fm}^2$ and $B(E2)$-values are in units of e^2fm^4, respectively. Both $B^W(M2)$ and $B^W(E2)$ relate to single-particle estimates in Weisskopf units, W.u.

4. Discussion

To interpret the refined and new results on isomeric states described in section 3, shell-model calculations have been performed based on the well-established KB3 and KB3G interactions [41–43] employing the full pf model space. Isospin-breaking terms both for the Coulomb and the nuclear part of the KB3 interaction as well as effective charges are probed on the $A = 43, 45$ negative-parity mirror isomers in section 4.1. Detailed polarization effects of nucleons moving in different orbitals outside the ^{40}Ca core are studied in section 4.2. This approach, which is different from standard shell-model calculations with a fixed set of effective charges has been triggered by recent experimental results in heavier pf-shell nuclei [44, 45] and introduced in detail in [46]. Section 4.3 provides first results on $M2$ mirror isomers using a restricted sdpf model space [47].

4.1. Isospin-breaking pf shell-model calculations

The shell-model calculations outlined in this section are performed with the code ANTOINE [48, 49]. Using the notations and descriptions introduced in [12, 14, 15], multipole harmonic-oscillator Coulomb matrix elements, V_{CM}, the monopole electromagnetic spin–orbit effect, V_{Cls}, and a repulsive 100 keV term for the $1f^2_{7/2}$, $J = 2$ two-proton matrix element, V_{BM}, are taken into account. The latter, charge-asymmetric component of the strong nucleon–nucleon interaction was suggested by [15] and supported by several measurements of specific energy differences of excited analogue states in pf-shell mirror nuclei (see, e.g., [50, 51] and [12] for a recent review). More recently, an investigation based on the observation of core excited $A = 54$ analogue states confirmed this $J = 2$ two-proton matrix element representing the most relevant isospin-breaking component [52]. Monopole-related shifts of single-particle energy levels, V_{Cr}, are treated along the prescription of [14].

This approach predicts, for example, the $19/2^-$ isomer in ^{43}Ti and ^{43}Sc at 2968 and 3058 keV excitation energy in the case of the KB3G interaction, to be compared with the measured 3066.4(1) and 3123.2(3) keV, respectively. Similarly, the calculations based on the KB3G interaction place the $3/2^-$ isomers in ^{45}V and ^{45}Ti at 185 keV and 174 keV, respectively. Excitation energies of 56.8(6) and 36.5(2) keV are known experimentally.

Effective g-factors have been chosen to correspond to free g-factors, and two sets of global pf effective charges have been used: the so-called standard pf-shell ones, $e_p = 1.5$ and $e_n = 0.5$, [42], and the ones derived experimentally from heavier $N \sim Z$ pf nuclei, $e_p = 1.15$ and $e_n = 0.80$, [44]. Potential orbital dependences of effective charges [45, 46] are discussed in the following section. The results concerning the states of interest in $A = 43$ and $A = 45$ mirror nuclei are summarized in table 2.

4.1.1. Transition rates. For the $A = 43$, $T_z = \pm 1/2$ mirror pair, the precisely measured lifetimes of the isomeric $19/2^-$ states provide the reduced transition strengths, $B(E2; 19/2^- \rightarrow 15/2^-)$, for both nuclei as well as the ratio of the two, $R = 4.78(10)/2.67(4) = 1.79(5)$. The aim for the model calculations is to reproduce all three experimental numbers, which define an experimental basis comparable to the preceding study of the $A = 51$ pair [44]. Similar to that, the shell-model wavefunctions of the concerned states comprise essentially pure, aligned $1f_{7/2}{}^3$ configurations, namely 90–95% for the initial $19/2^-$ and some 75% for the final $15/2^-$ state. These partitions are also quite stable for any modern pf-shell

Table 2. Comparison of experimental and calculated electromagnetic properties associated with selected $A = 43$ and $A = 45$ negative-parity states. Effective charges are standard values [42] or derived from measured lifetimes in $A = 51$ mirror nuclei, $e_p = 1.15$, $e_n = 0.80$ [44]. Numbers without plus or minus signs on static moments indicate absolute experimental values. For spin-parity values, parantheses denote tentative experimental assignments. The square brackets used for ^{45}Cr imply a case study, i.e. assuming an $I^\pi = 3/2^-$ assignment of the isomeric state observed in ^{45}Cr.

				$B(E2)$ (W.u.)					
				Experimental	KB3		KB3G		
	E_γ	I_i^π	I_f^π	from	$e_p = 1.5$	$e_p = 1.15$	$e_p = 1.5$	$e_p = 1.15$	$e_p = 1.20$
	(keV)	($\hbar$)	($\hbar$)	table 1	$e_n = 0.5$	$e_n = 0.80$	$e_n = 0.5$	$e_n = 0.80$	$e_n = 0.55$
^{43}Sc	136	$19/2^-$	$15/2^-$	2.67(4)	3.13	3.99	3.07	3.94	2.67
^{43}Ti	115	$(19/2^-)$	$(15/2^-)$	4.78(10)	7.11	5.36	7.07	5.30	4.94
^{45}Sc	377	$3/2^-$	$7/2^-$	15(1)	11.4	15.4	12.0	16.0	10.6
^{45}Ti	37	$3/2^-$	$7/2^-$	17(2)	12.8	13.5	13.4	14.1	10.7
^{45}V	57	$(3/2^-)$	$7/2^-$	22(5)	17.5	15.0	17.9	15.4	13.2
^{45}Cr	107	$[3/2^-]$	$7/2^-$	< 0.05	29.6	21.6	30.1	22.2	20.9
	E_x	I^π			Q (eb)			μ (μ_N)	
	(keV)	($\hbar$)		exp [37, 53]	KB3[a]	KB3G[a]		exp [37, 53]	KB3	KB3G
^{43}Sc	0	$7/2^-$		$-0.26(6)$	-0.17	-0.18		+4.62(4)	+4.63	+4.74
	3123	$19/2^-$		0.199(14)	-0.23	-0.22		+3.122(7)	+3.64	+3.15
^{43}Ti	0	$7/2^-$			-0.20	-0.21		0.85(2)	-0.73	-0.83
	3066	$(19/2^-)$		0.30(7)	-0.26	-0.24		+7.22(1)	+6.58	+7.28
^{45}Sc	0	$7/2^-$		$-0.22(1)$	-0.20	-0.20		+4.756487(2)	+4.83	+4.81
		$3/2^-$			-0.11	-0.11			+3.63	+3.68
^{45}Ti	0	$7/2^-$		0.015(15)	-0.081	-0.085		0.095(2)	-0.38	-0.25
	37	$3/2^-$			+0.15	+0.15			-0.46	-0.35
	39	$5/2^-$			-0.077	-0.070		$-0.133(1)$	-0.23	-0.29
^{45}V	0	$7/2^-$			-0.12	-0.11			+4.23	+4.12
	57	$(3/2^-)$			+0.16	+0.16			+2.17	+2.03
	57	$(5/2^-)$			-0.094	-0.082			+2.89	+3.03
^{45}Cr	0	$7/2^-$			-0.25	-0.25			-0.91	-0.90
	107	$[3/2^-]$			-0.14	-0.14			-1.80	-1.93

[a] Using $e_p = 1.20$, $e_n = 0.55$.

interaction. This becomes apparent, for instance, when comparing corresponding transition rates for KB3 and KB3G in table 2.

Despite the anticipated simplicity of the involved nuclear states and the overall success of the present type of shell-model calculations describing detailed nuclear structure in the pf shell, neither the standard set nor the refined set of effective charges is able to reproduce the $B(E2)$ values and their ratio of the $A = 43$ mirror system at the same time: with $e_p = 1.5$, $e_n = 0.5$ the calculated $B(E2)$ strength is in very good agreement with the experimental number for ^{43}Sc, but fails for ^{43}Ti and, consequently, for the ratio, R. The situation is vice versa for the choice $e_p = 1.15$, $e_n = 0.80$. As illustrated in the rightmost column of table 2, the experimental values can be very well reproduced using the combination $e_p = 1.20$, $e_n = 0.55$ in the case of the KB3G interaction (and, similarly, for KB3). These numbers are consistent with an early investigation outlined in [8], while stressing the rather pure $1f_{7/2}{}^3$ configurations of the states of interest.

A glance at the $A = 45$-related numbers in table 2 reveals that these optimum values of effective charges derived for the $A = 43$ mirror nuclei provide the least accurate prediction, namely underestimate the $B(E2; 3/2^- \rightarrow 7/2^-)$ strengths by about one third. Secondly, the experimental uncertainties of the $A = 45$, $T_z = \pm 1/2$ mirror system prohibit any firm preference of combination of effective charges. Both established sets provide about equally good overall descriptions of the experimental data, while calculations using the standard values of e_p and e_n only yield a somewhat more consistent description of the increasing trend of transition rates from ^{45}Sc via ^{45}Ti towards ^{45}V. Nevertheless, $e_p + e_n \gtrsim 2$ can be justified. Last but not least, the new state at 107 keV in ^{45}Cr cannot be associated with the lowest predicted $3/2^-$ state, since its long experimental half-life is inconsistent with the predictions as well as expectations from isospin symmetry by at least two orders of magnitude.

With $e^{(0)}_{\rm pol}$ and $e^{(1)}_{\rm pol}$ denoting the isoscalar and isovector contributions arising from excitations of giant quadrupole resonances, respectively,

$$e_p = 1 + e^{(0)}_{\rm pol} - e^{(1)}_{\rm pol} \quad \text{and} \quad e_n = e^{(0)}_{\rm pol} + e^{(1)}_{\rm pol}. \tag{3}$$

While the results in [44] ($e^{(0)}_{\rm pol} \sim 0.47$, $e^{(1)}_{\rm pol} \sim 0.32$) are consistent with expectations for $N \sim Z$ nuclei [54], the more recent measurements on neutron-rich ^{50}Ca and ^{51}Sc indicate vanishing isovector contributions, $e^{(1)}_{\rm pol} \sim 0$, for states dominated by $2p_{3/2}$ configurations [45]. Here, trying to reproduce the experimental values for $A = 43$, $T_z = \pm 1/2$ nuclei calls for a reduced isoscalar ($e^{(0)}_{\rm pol} \sim 0.38$) and halved isovector ($e^{(0)}_{\rm pol} \sim 0.17$) contribution.

Possible approaches of solving this apparent puzzle are, for example, the use of more realistic potentials, which may provide state and/or orbital-dependent mean square radii. Note that transition probabilities derived from (large-scale) shell-model calculations are typically based on well-confined harmonic oscillator wavefunctions. In addition, proton wavefunctions dominated by low-j orbitals in $N < Z$ nuclei may give further rise to increased charge radii or, at least, different charge radii of analogue states in mirror pairs. Recently, an orbital dependence of effective charges has been discussed in [45], and more recently, first attempts towards state-dependent predictions have been put forward [46]. Section 4.2 provides an application of the underlying model on the presently investigated $A = 43$ and $A = 45$ mirror nuclei.

4.1.2. Static moments. The lower part of table 2 summarizes the limited experimental knowledge on static electric quadrupole and magnetic dipole moments of the selected nuclei in the lower part of the pf shell. In particular the magnetic dipole moments of the $A = 43$ mirror nuclei as well as the ground state of the stable isotope ^{45}Sc are extremely well reproduced with

the KB3G parameter set with less than 3% deviation between experiment and theory. KB3 performs only slightly worse.

The shell-model calculations provide spectroscopic quadrupole moments [48, 49]. Both interactions yield about equally good levels of agreement in describing the electric quadrupole moments of four of these five states of interest; the electric quadrupole moment of the $7/2^-$ ground state of ^{43}Ti has not been measured yet. Based on the discussion on the transition rates above, the predictions are based on $e_p = 1.20$ and $e_n = 0.55$. However, the use of the standard effective charges or those derived in [44] does not alter the picture. For example, $Q = -0.22$ and $Q = -0.24$ are calculated for the ground state of ^{43}Ti, respectively, instead of $Q = -0.21$ in table 2. Furthermore, looking at the experimental and predicted values of electric quadrupole moments of mirror states, it becomes evident that this variable is rather insensitive to isospin breaking effects—at the same time it is a quantity which is rather difficult to measure.

By contrast, transition rates and magnetic dipole moments are more promising to study details of the isospin degree of freedom. There are, for example, distinct differences of both ground and excited mirror states, both predicted and measured.

A final note concerns the rather old measurements of moments of the ground and excited states quoted for ^{45}Ti [53]. Given the level of agreement for all other states, which have been derived with in part much higher precision, an experimental revision appears more of a concern than trying to assess possible reasons for the discrepancy with the present predictions.

4.2. State-dependent effective charges

The investigation of dynamic and static electric moments in section 4.1 is based on a single set of effective charges for the full pf shell and harmonic oscillator wavefunctions. Recent experimental results on neutron rich pf-shell nuclei indicate, however, an orbital dependence of effective charges [45]. Therefore, the approach of deriving microscopically state- and orbital-dependent effective charges [46] is employed to assess the present results from that point of view as well.

In [46], the method estimates the $B(E2)$ values of the terminating bands in Ti isotopes. In the cases concerned, the microscopic effective charges as well as the standard charges $e_p = 1.5$, $e_n = 0.5$ both well reproduce the experimental $B(E2)$ values for terminating states, for which the valence particles tend to converge in $1f_{7/2}$ orbitals. Hence, the $B(E2)$ values of terminating states become superior probes for the effective charges related in particular to $1f_{7/2} \rightarrow 1f_{7/2}$ dominated transitions. Indeed, this is similar to the aligned $19/2^-$ mirror states in ^{43}Ti and ^{43}Sc, respectively.

The microscopic polarization charges are calculated in the framework of the particle-vibration coupling model, where the giant quadrupole resonances are treated by the continuum random phase approximation on top of the Skyrme Hartree–Fock (HF) mean field. Based on the one-body transition densities given by the shell-model calculations, the electric quadrupole transition matrix elements are calculated by two methods. The one labelled as PV in table 3 uses the microscopic polarization charges and the Skyrme HF wavefunctions. Here, the HF wavefunctions using the SKM* interaction [55] are applied to estimate polarization charges as well as estimate reduced matrix elements when calculating $B(E2)$ values. The other method labelled as HO uses the standard effective charges, $e_p = 1.5$ and $e_n = 0.5$, with harmonic oscillator wavefunctions, similar to the calculations in section 4.1 but without considering explicit isospin breaking terms. In the HO method the oscillator parameter $\hbar\omega \approx 45A^{-1/3} - 25A^{-2/3}$ ($b = \sqrt{41.46/(\hbar\omega)}$) [56] is applied. A denotes the mass number.

Table 3. Calculated microscopic effective charges, e_p and e_n, of $1f_{7/2} \rightarrow 1f_{7/2}$ and $2p_{3/2} \rightarrow 1f_{7/2}$ transitions and predicted $B(E2)$ reduced transition strength for isomeric mirror states in the lower-pf shell. Calculations in the harmonic oscillator basis use the standard effective charges $e_p = 1.5$ and $e_n = 0.5$ for reference. See the text for details.

	e_p	e_n	e_p	e_n		$B(E2)$ (W.u.)			$\langle r_p^2\rangle^{\frac{1}{2}}$ (fm)		$\langle r_n^2\rangle^{\frac{1}{2}}$ (fm)	
	$1f_{7/2} \rightarrow 1f_{7/2}$		$2p_{3/2} \rightarrow 1f_{7/2}$		$I_i^\pi(\hbar)$	Experimental	HO	PV	HO	HF	HO	HF
^{43}Sc	1.34	0.61	1.32	0.56	$19/2^-$	2.67(4)	2.80	2.78	3.43	3.47	3.47	3.45
^{43}Ti	1.36	0.66	1.33	0.63	$19/2^-$	4.78(10)	6.67	6.11	3.47	3.50	3.43	3.42
^{45}Sc	1.32	0.57	1.32	0.52	$3/2^-$	15(1)	11.2	10.0	3.45	3.48	3.55	3.51
^{45}Ti	1.32	0.60	1.32	0.56	$3/2^-$	17(2)	12.9	11.9	3.49	3.52	3.52	3.49
^{45}V	1.35	0.66	1.34	0.64	$3/2^-$	22(5)	17.7	17.1	3.52	3.56	3.49	3.46
^{45}Cr	1.38	0.73	1.36	0.73	$[3/2^-]$	< 0.05	28.8	28.8	3.55	3.59	3.45	3.43

The NuShell@MSU code [57] with the full pf shell and the KB3 [26, 42] residual interaction was used. Table 3 provides the state-dependent effective charges for the most relevant $1f_{7/2} \rightarrow 1f_{7/2}$ and $2p_{3/2} \rightarrow 1f_{7/2}$ transitions, the predicted $B(E2)$ values calculated with the PV and HO methods, as well as the proton and neutron root-mean square radii. These radii of initial states are calculated by combining the one-body transition densities, i.e. in the present case the occupation numbers in the valence orbitals, with the HO or HF single-particle wavefunctions.

The differences for proton and neutron radii of the states of interest in table 3 appear to be small on the few percent level. Since all pf orbitals have non-zero orbital momentum and in view of the Coulomb barrier, the HO wavefunctions are certainly a good approximation even for protons at the surface of neutron-deficient nuclei. For deeply bound neutrons, the HO wavefunction is a good approximation, too. Thus it is in principle safe to use HO wavefunctions even for nuclei close to the proton drip line. Nevertheless, different differences of neutron and proton radii of isobaric analogue states do have an impact on electromagnetic observables of mirror states—and even their relative excitation energies by means of different Coulomb energy shifts as discussed, for instance, in [12, 14].

The microscopic effective charges for $1f_{7/2} \rightarrow 1f_{7/2}$ transitions are found to be approximately $e_p \sim 1.35$ and $e_n \sim 0.65$ for both $A = 43$ and $A = 45$ nuclei, respectively, under investigation. The values for $2p_{3/2} \rightarrow 1p_{7/2}$ transitions are similar. These numbers are also consistent with the experimentally extracted values in [8], at that time assuming a simple, restricted $1f_{7/2}{}^n$ shell-model space.

The values $e_p \sim 1.35$ and $e_n \sim 0.65$ imply isoscalar $e_{\rm pol}^{(0)} \sim 0.50$ and isovector $e_{\rm pol}^{(1)} \sim 0.15$ charges, the latter being similar to the one derived in section 4.1 but different from the values indicated in [44, 45]. Note that the PV method provides an improved description of the $B(E2; 19/2^- \rightarrow 15/2^-)$ rate in ^{43}Ti and, consequently, the ratio of the decay strengths of the corresponding $A = 43$ mirror states. One reason is the larger difference of calculated proton and neutron radii for the PV compared to the HO method for ^{43}Ti.

The microscopic effective charges show some isospin dependence: the values increase as isospin $T_z = (N - Z)/2$ values decrease, and more pronounced for e_n (some 25%) than for e_p (some 5%) when moving from ^{45}Sc ($T_z = 3/2$) to ^{45}Cr (T_z =-3/2). The effective charges between other pf orbitals are somewhat reduced with respect to the values of the $1f_{7/2} \rightarrow 1f_{7/2}$ transition, because these orbitals are further away from the nuclear surface for nuclei in the lower part of the $1f_{7/2}$ shell.

Table 4. Some $B(M2)$ reduced transition strengths of $3/2^+ \rightarrow 7/2^-$ yrast transitions for mirror nuclei in the lower pf shell predicted by sdpf shell-model calculations.

	E_γ (keV)	I_i^π ($\hbar$)	I_f^π ($\hbar$)	$B(M2)$ (W.u.) Experimental	sdpf
^{43}Sc	152	$3/2^+$	$7/2^-$	0.069(2)	0.064
^{43}Ti	313	$(3/2^+)$	$7/2^-$	0.071(2)	0.154
^{45}Sc	12.4	$3/2^+$	$7/2^-$	$0.042(^{10}_{6})$	0.047
^{45}Cr	107	$(3/2^+)$	$7/2^-$	< 1.9	0.106

In table 3 it is shown that the PV and HO methods reproduce the $B(E2)$ values of terminating states in ^{43}Sc and ^{43}Ti to about the same extent. However, for the $3/2^- \rightarrow 7/2^-$ transitions, both methods underestimate the $B(E2)$ values. This kind of underestimation can also be seen at low spins in other pf-shell nuclei, for example in ^{48}Cr [26] or ^{46,48}Ti [46]. Further theoretical investigations of these low-lying states appear necessary, possibly including 2p–2h excitations across the shell gap at particle number 20.

4.3. First assessment of M2 mirror isomers

In [19], positive-parity bands in some odd-A pf-shell nuclei were discussed in the framework of an extended shell-model space. In particular, reported $3/2^+$ states in several odd-A nuclei in the lower part of the $1f_{7/2}$ shell are well described by a dominant $1d_{3/2}$ character. In this paper, the $A = 43$ and $A = 45$ $I^\pi = 3/2^+$ mirror isomers in ^{43}Sc and ^{43}Ti as well as ^{45}Sc and ^{45}Cr are calculated with a sdpf interaction based on [47], but with some monopole modifications according to [58]. This interaction is part of the NuShell@MSU package [57]. Note that this interaction does not include any monopole- or multipole-related isospin-breaking terms.

In the present calculation, the $1d_{5/2}$ and $2s_{1/2}$ orbitals are fully occupied and closed as set in [47]. The $B(M2)$ strengths are evaluated with free g-factors and harmonic oscillator wavefunctions. The calculated reduced $B(M2)$ transition strengths are compared with the experimental values in table 4. Clearly, the predictions fall into the right order of magnitude of $B(M2) \sim 0.05$-0.10 W.u., with the experimental numbers of the neutron-rich partners, namely ^{43,45}Sc, being very well reproduced. The mismatch of about a factor of 2 in the case of ^{43}Ti can possibly be linked to the necessity of either including isospin-breaking terms in the interaction or modifying the effective g-factors for $M2$ transitions. A detailed investigation of these effects, however, requires a dedicated theoretical study on a broader basis of experimental states in the vicinity of doubly-magic $N = Z = 20$ ^{40}Ca. Including the $1d_{5/2}$ and $2s_{1/2}$ orbitals in the shell-model calculations simply quenches the $B(M2)$ transition strengths in ^{43}Sc and ^{43}Ti to 0.058 W.u. and 0.093 W.u., respectively.

Last but not the least, the prediction of $B(M2) = 0.106$ W.u. for the $= 3/2^+ \rightarrow 7/2^-$ transition in ^{45}Cr provides confidence in associating the observed isomeric state in ^{45}Cr with this calculated state. With respect to section 4.1, a $3/2^-$ assignment appears highly unlikely due to severe inconsistencies with both the pf shell-model calculations and isospin symmetry arguments. Using the ratio of the observed upper limit and the predicted $B(M2)$ value, a halflife on the order of 1–2 ms can be estimated for a likely $3/2^+$ state at 107 keV excitation energy.

5. Summary

Isomeric states in the neutron-deficient mass $A = 43$ and $A = 45$ isotopes have been observed using the GSI fragment separator in combination with the RISING Ge-detector

array. The electromagnetic properties of isomeric states in mirror nuclei are interpreted based on shell-model calculations. The microscopic particle-vibration coupling model on top of the selfconsistent Skyrme HF plus continuum random phase approximation theory is used to estimate the core polarization charges.

A previously unreported isomeric γ-ray transition of 107 keV energy in T_z =-3/2 ^{45}Cr is interpreted as a $3/2^+ \rightarrow 7/2^-$ $M2$ decay. This is in line with previous experimental findings on this exotic isotope [38]. Corresponding $A = 43$ and $A = 45$ $B(M2; 3/2^+ \rightarrow 7/2^-)$ transition rates are very well described by contemporary sdpf shell-model calculations.

The present results add further evidence that pairs of mirror nuclei between $N = Z = 20$ and $N = Z = 28$ are prime candidates to study subtle effects of isospin-breaking forces, which alter notably shell-model interactions and thus their predictions. Here, lifetime measurements with the deduced transition strengths as well as magnetic dipole moments provide more profound testing grounds than static electric quadrupole moments.

In view of the present experimental results and the studies of [44–46] it is apparent that state- and orbital-dependent effective charges are needed to explain all observed $B(E2)$ transition rates in pf-shell nuclei. This concerns mostly the isovector components of the effective charges, which seemingly differ for nuclei near ^{56}Ni, $e^{(1)}_{\rm pol} \sim 0.35$ [44], ^{48}Ca, $e^{(1)}_{\rm pol} \sim 0$ [45] and ^{40}Ca, $e^{(1)}_{\rm pol} \sim 0.15$ (present study).

Whether or not extended radii of protons in valence orbitals of states in nuclei near the proton dripline are crucial to include in these investigations remains to be seen. Of course, measurements of charge distributions of ground and isomeric states in unstable (mirror) nuclei are decisive and on the horizon at upcoming radioactive ion-beam facilities.

Acknowledgments

The authors gratefully acknowledge the outstanding work of the GSI accelerator and ion-source crews in providing the experiments with the envisaged high beam intensities. This work is supported by the European Commission contract no 506065 (EURONS), the Swedish Research Council, STFC (United Kingdom), the German BMBF, grant 06KY205I, the Polish Ministry of Science and Higher Education, under grants NN 202 109936 and NN 202 309135, the Bulgarian Science Fund, VUF06/05, the Spanish science council, and the US Department of Energy grants DE-FG02-91ER-40609 and W-31-109-ENG-38.

References

[1] Walker P and Dracoulis G 1999 *Nature* **399** 35
[2] Jungclaus A *et al* 2007 *Phys. Rev. Lett.* **99** 132501
[3] Garnsworthy A B *et al* 2008 *Phys. Lett.* B **660** 326
Garnsworthy A B *et al* 2008 *Phys. Lett.* B **668** 460 erratum)
[4] Garnsworthy A B *et al* 2009 *Phys. Rev.* C **80** 064303
[5] Regan P H *et al* 2007 *Nucl. Phys.* A **787** 491c
[6] Rudolph D *et al* 2007 *Eur. Phys. J. Special Topics* **150** 173
[7] Häusser O, Alexander T K, Faestermann T, Horn D, Ward D, Andrews H R and Towner I S 1978 *Phys. Lett.* B **73** 127
[8] Dafni E, Mahnke H E, Noé J W, Rafailovich M H and Sprouse G D 1981 *Phys. Rev.* C **23** 1612
[9] Meyer-Schützmeister L, Elwyn A J, Gronemeyer S A, Hardie G, Holland R E and Rehm K E 1978 *Phys. Rev.* C **18** 1148
[10] Gronemeyer S A, Meyer-Schützmeister L, Elwyn A J and Hardie G 1980 *Phys. Rev.* C **21** 1290
[11] Mueller D, Kashy E and Benenson W 1977 *Phys. Rev.* C **15** 1282
[12] Bentley M A and Lenzi S M 2007 *Prog. Part. Nucl. Phys.* **59** 497

[13] Andersson L-L, Johansson E K, Ekman J, Rudolph D, du Rietz R, Fahlander C, Gross C J, Hausladen P A, Radford D C and Hammond G 2005 *Phys. Rev.* C **71** 011303
[14] Ekman J, Fahlander C and Rudolph D 2005 *Mod. Phys. Lett.* A **20** 2977
[15] Zuker A P, Lenzi S M, Martinez-Pinedo G and Poves A 2002 *Phys. Rev. Lett.* **89** 142502
[16] Johansson E K *et al* 2006 *Eur. Phys. J.* A **27** 157
[17] Minamisono K *et al* 2006 *Phys. Rev. Lett.* **96** 102501
[18] Rudolph D *et al* 2008 *Eur. Phys. J.* A **36** 131
[19] Poves A and Sánchez Solano J 1998 *Phys. Rev.* C **58** 179
[20] Stoitcheva G, Satula W, Nazarewicz W, Dean D J, Zalewski M and Zduńczuk H 2006 *Phys. Rev.* C **73** 061304
[21] Bentley M A *et al* 2006 *Phys. Rev.* C **73** 024304
[22] Chiara C J *et al* 2007 *Phys. Rev.* C **75** 054305
[23] Rudolph D *et al* 1999 *Phys. Rev. Lett.* **82** 3763
[24] Ekman J *et al* 2002 *Phys. Rev.* C **66** 051301
[25] Caballero O L, Cristancho F, Rudolph D, Baktash C, Devlin M, Riedinger L L, Sarantites D G and Yu C-H 2003 *Phys. Rev.* C **67** 024305
[26] Caurier E, Martínez-Pinedo G, Nowacki F, Poves A and Zuker A P 2005 *Rev. Mod. Phys.* **77** 427
[27] Geissel H *et al* 1992 *Nucl. Instrum. Methods* B **70** 286
[28] Hoischen R *Master Thesis* Lund University, unpublished
[29] Montuenga P *Master Thesis* Lund University, unpublished
[30] Eberth J, Thomas H G, von Brentano P, Lieder R M, Jäger H M, Kämmerling H, Berst M, Gutknecht D and Henck R 1996 *Nucl. Instrum. Methods* A **369** 135
[31] Pietri S *et al* 2007 *Nucl. Instrum. Methods* B **261** 1079
Pietri S *et al* 2007 *Acta Phys. Pol.* B **38** 1255
[32] Iordăchescu A, Ivanov E A and Pascovici G 1974 *Phys. Lett.* **48B** 28
[33] van Driel M A, Eggenhuisen H H, Hermans J A J, Bucurescu D, van Rinsvelt H A and Engelbertink G A P 1974 *Nucl. Phys.* A **226** 326
[34] Morozov A M and Remaev V V 1963 *Sov. Phys.—JETP* **16** 314
[35] Conlon T W 1967 *Phys. Lett.* B **24** 661
[36] Cameron J A and Singh B 2001 *Nucl. Data Sheets* **92** 783
[37] Burrows T W 2008 *Nucl. Data Sheets* **109** 171
[38] Dossat C *et al* 2007 *Nucl. Phys.* A **792** 18
[39] Kibédi T, Burrows T W, Trzhaskovskaya M B, Davidson P M and Nestor C W Jr 2008 *Nucl. Instrum. Methods* A **589** 202
[40] Morinaga H and Yamazaki T 1976 *In-Beam Gamma-Ray Spectroscopy* (Amsterdam: North-Holland)
[41] Kuo T T S and Brown G E 1968 *Nucl. Phys.* A **114** 241
[42] Poves A and Zuker A P 1981 *Phys. Rep.* **70** 235
[43] Poves A, Sánchez-Solano J, Caurier E and Nowacki F 2001 *Nucl. Phys.* A **694** 157
[44] du Rietz R *et al* 2004 *Phys. Rev. Lett.* **93** 222501
[45] Valiente Dobón J J *et al* 2009 *Phys. Rev. Lett.* **102** 242502
[46] Ma H L, Dong B G, Yan Y L and Zhang X Z 2009 *Phys. Rev.* C **80** 014316
[47] Nummela S *et al* 2001 *Phys. Rev.* C **63** 044316
[48] Caurier E 1989-2002 Shell model code `ANTOINE`, IRES, Strasbourg
[49] Caurier E and Nowacki F 1999 *Acta Phys. Pol.* B **30** 705
[50] Williams S J *et al* 2003 *Phys. Rev.* C **68** 011301
[51] Gadea A *et al* 2006 *Phys. Rev. Lett.* **97** 152501
[52] Rudolph D *et al* 2008 *Phys. Rev.* C **78** 021301
[53] Stone N J 2005 *At. Data Nucl. Data Tables* **90** 75
[54] Bohr A and Mottelson B R 1975 *Nuclear Structure* vol 2 (New York: Benjamin) chapter 6
[55] Bartel J, Quentin P, Brack M, Guet C and Hakansson H B 1982 *Nucl. Phys.* A **386** 79
[56] Blomqvist J and Molinari A 1968 *Nucl. Phys.* A **106** 545
[57] Brown B A and Rae W D M 2007 *MSU-NSCL Report*
[58] Retamosa J, Caurier E, Nowacki F and Poves A 1997 *Phys. Rev.* C **55** 1266